Raman dispersion spectroscopy probes heme distortions in deoxyHb-trout IV involved in its T-state Bohr effect

Reinhard Schweitzer-Stenner, Michael Bosenbeck, and Wolfgang Dreybrodt
Institute of Experimental Physics, University of Bremen, 2800 Bremen 33, Germany

ABSTRACT The depolarization ratios of heme protein Raman lines arising from vibrations of the heme group exhibit significant dependence on the excitation wavelength. From the analysis of this depolarization ratio dispersion, one obtains information about symmetry-lowering distortions δQ^{Γ} of the heme group that can be classified in terms of the symmetry races $\Gamma = A_{1g}$, B_{1g}, B_{2g}, and A_{2g} in D_{4h} symmetry. The heme-protein interaction can be changed by the protonation of distinct amino acid side chains (i.e., for instance the Bohr groups in hemoglobin derivates), which gives rise to specific static heme distortions for each protonation state. From the Raman dispersion data, it is possible to obtain parameters by fitting to a theoretical expression of the Raman tensor, which provide information on these static distortions and also about the pK values of the involved titrable side chains. We have applied this method to the ν_4 (1,355 cm^{-1}) and ν_{10} (1,620 cm^{-1}) lines of deoxygenated hemoglobin of the fourth component of trout and have measured their depolarization ratio dispersion as a function of pH between 6 and 9. From the pH dependence of the thus derived parameters, we obtain pK values identical to those of the Bohr groups, which were earlier derived from the corresponding O_2-binding isotherms. These are $pK_{\alpha 1} = pK_{\alpha 2} = 8.5$ for the α and $pK_{\beta 1} = 7.5$, $pK_{\beta 2} = 7.4$ for the β chains. We also obtain the specific distortion parameters for each protonation state. As shown in earlier studies, the ν_4 mode mainly probes distortions from interactions between the proximal histidine and atoms of the heme core (i.e., the nitrogens and the C_α atoms of the pyrroles). Group theoretical argumentation allows us to relate specific changes of the imidazole geometry as determined by its tilt and azimuthal angle and the iron-out-of-plane displacement to distinct variations of the normal distortions δQ^{Γ} derived from the Raman dispersion data. Thus, we found that the pH dependence of the heme distortions δQ^{A1g} (totally symmetric) and δQ^{B1g} (asymmetric) is caused by variations of the azimuthal rather than the tilt angle of the Fe-His (F8) bond. In contrast to this, the ν_{10} line mainly monitors changes resulting from the interaction between peripheral substituents of the porphyrin macrocycle (vinyl). From the pH dependence of the parameters, it is possible to separately identify distortions δQ^{Γ} affecting the hemes in the α and β chains, respectively. From this, we find that in the α subunit structural changes induced on protonation of the corresponding Bohr groups are mainly transferred via the Fe—N_ϵ bond and give rise to changes in the azimuthal angle. In the β subunit, however, in addition, structural changes of the heme pocket arise, which most probably result from protonation of the imidazole of the COOH-terminal His (HC3 β). This rearranges the net of H bonds between His HC3 β, Ser (F9 β), and Glu (F7 β).

INTRODUCTION

The understanding of the molecular basis of the functionally relevant allosteric mechanism (i.e., cooperativity, Bohr and Root effect) in hemoglobin (Hb)[1] molecules is one of the major goals of the research work dedicated to these proteins. Numerous experimental and theoretical studies have provided substantial insight into the basic mechanism governing cooperativity of ligand binding to various Hb derivates (1–13). Our knowledge about the processes that transduce structural changes induced by proton binding to amino acid residues involved in the Bohr (14, 15) or Root effect (16), however, is still rather limited (17–19). Proton binding to Bohr groups, for example, may influence the apparent oxygen affinity of Hb by two different processes. It either changes the equilibrium between the low affinity tertiary t and the high affinity tertiary r state or directly affects the ligand affinity of the heme within a given t or r state (1, 2, 10). Whereas in the former case the heme groups in the deoxygenated (deoxy)Hb-t and oxygenated (oxy)Hb-r subunits remain unaffected by pH, some structural changes of prosthetic groups can be expected to occur in the latter case.

Such distortions of the active sites can be detected by resonance Raman dispersion spectroscopy (RDS) (20). It involves the measurement of polarized resonance excitation profiles (REPs) of Raman lines arising from skeletal modes of the porphyrin in the region between the B and Q absorption bands. From these data the corresponding depolarization ratio dispersion (DPD) can be derived. The latter reflects asymmetric distortions of the porphyrin macrocycle caused by the peripheral substituents attached to its β carbons and various noncovalent heme-protein interactions (3, 21–24). An analysis of these data in terms of an earlier derived theory on Raman scattering in the weak coupling regime (20) yields vibronic coupling parameters that depend on symmetry classified normal distortions of the heme. Proton binding to amino acid side chains may cause changes in the protein conformation that are transferred to the heme moiety, thus giving rise to distortions of the heme group specific to each titration state. In this case the total scattered Raman intensity has to be considered as an incoher-

[1] *Abbreviations used in this article:* CTT, chironomous thummi thummi; deoxyHbA, deoxygenated human hemoglobin; deoxyHb-trout IV, deoxygenated hemoglobin of the fourth component of trout; DPD, depolarization ratio dispersion; DPR, depolarization ratio; Hb, hemoglobin; HbA, human hemoglobin; HLC model, Heme–ligand coupling model; oxyHbA, oxygenated human hemoglobin; oxyHb-trout IV, oxygenated hemoglobin of the fourth component of trout; REP, resonance excitation profile; RTC, Raman titration curve; Tris, tris(hydroxymethyl)-aminomethane.

Address correspondence to Dr. Reinhard Schweitzer-Stenner, Institute of Experimental Physics, University of Bremen, 2800 Bremen 33, Germany.

0006-3495/93/04/1194/16 $2.00

ent superposition of the scattering at proteins existing in different titration states, the concentration of which is determined by pH, and the pK values of the above side chains. As a consequence the DPD becomes pH dependent, and the pK value of the distorting protonation processes can be derived by analyzing the pH dependence of the corresponding effective vibronic coupling parameters (20).

As previously shown, RDS can be applied successfully to elucidate various aspects of allosteric interactions between protein binding sites and the porphyrin macrocycle in Hb molecules (20). To this end, we measured the DPDs of the oxidation marker line ν_4 and the spin marker line ν_{10} of their Raman spectra. For human hemoglobin (HbA), we found that protonation of Bohr groups (i.e., for instance the COOH-terminal His HC3 β) induces significant symmetry-lowering distortions of the heme groups in oxyHbA (19), whereas deoxyHbA remains unaffected (24). On the other hand, it is known that all the corresponding Adair constants depend on pH (25), indicating that the Bohr effect is operative in the T and R state of the protein. Thus, our results suggest that the mechanisms governing the Bohr effect are different in the quaternary states T and R. The T-state Bohr effect changes mainly the equilibrium between the t and r states of the subunits (i.e., proton binding stabilizes t), whereas the R-state Bohr effect directly affects the conformation of the ligated r state (18, 19). RDS experiments on oxyHbA derivatives (26–28) suggest that in the R-state Bohr effect, allosteric coupling mechanisms are involved in the β rather than in the α subunits. This is corroborated by earlier time-resolved Raman experiments on photodissociated HbA hybrids $\alpha(\mathrm{Fe})_2^* \beta(\mathrm{Co})_2$ and $\alpha(\mathrm{Co})_2 \beta(\mathrm{Fe})_2^*$ that revealed different time dependences of the apparent frequency of the structural sensitive Fe—N_ϵ (His F8)-stretching mode at different pH on relaxation of the protein structure after photolysis (17, 29). Although the relaxation into the deoxygenated T state was found to be pH independent for the α subunits, it exhibits a considerable pH dependence for the β subunits. Moreover, RDS experiments on isolated oxy-HbA chains revealed that the DPDs of the oxidation and spin marker lines ν_4 and ν_{10} of the β chain vary as a function of pH, whereas the corresponding DPDs of the α chain are pH independent (30). In the physiological relevant region between pH 6 and 9, distorting interactions between proton binding sites and heme groups seem to be confined to those amino acid residues that are involved in the allosteric linkage between proton and ligand binding (i.e., Bohr and Root groups) (1, 2, 5, 10, 16, 31, 32). If the latter is absent as is the case, for example, in myoglobin (33) and Hb-BME (bis(*N*-maleimidodimethyl)ether; cf. reference 34), the DPDs of the corresponding ν_4 and ν_{10} lines are found to be pH independent between 6 and 8 (26, 27, 35, 36).

Recently, we also investigated the influence of proton binding to the structure of oxyHb of the fourth component of trout (oxyHb-trout IV). This particular Hb molecule is of considerable interest because its binding isotherms for O_2 and CO indicate a complete breakdown of cooperativity at pH below 6.5 (Root effect) (16, 32, 37, 38). The analysis of these binding curves for various pH between 6.1 and 7.7 (16, 37) by virtue of an extended Herzfeld–Stanley model (2) reveals that the fully oxygenated molecule undergoes a conformational R → T transition on lowering the pH below 7.0 (39). This can be understood in terms of proton binding to yet unidentified amino acid residues (Root groups), which lower the free energy of cooperativity by stabilizing the quarternary T state. In addition, proton binding to Bohr groups lowers the apparent ligand affinity at pH above 7.0.

The deoxygenated molecule of Hb-trout IV is in the T state, and all its subunits exhibit their tertiary structures in the t state, independent of pH. In contrast to what has been found for HbA, the Bohr effect in Hb-trout IV depends on the nature of the ligand (16, 32, 37). This indicates that in contrast to what has been observed for HbA, the Bohr effect of Hb-trout IV operates by direct coupling between proton and ligand binding sites (2, 39). Consequently, one expects that this type of allosteric interaction is involved in both, the T- and R-state Bohr effect of Hb-trout IV.

To investigate the corresponding allosteric coupling mechanism, RDS was first applied to oxyHb-trout IV at pH between 6.7 and 8.5. From the pH dependence of the vibronic coupling parameters determining the Raman intensity of the ν_4 mode, we found that in particular the protonation of the Root groups cause a considerably strong asymmetric B_{1g}-type perturbation of the pyrrole nitrogen N(III) of the porphyrin macrocycle (Fig. 1) in the β subunits. The underlying mechanism involves the r → t transition of the ligated β subunits that forces the imidazole of the corresponding proximal His F8 into a more tilted position with respect to the heme normal, thus increasing repulsive interactions between C_ϵ of the imidazole and N(III) of the heme. The α subunits do not exhibit these conformational changes because the quaternary transition is not capable to switch their tertiary structures from r → t in the fully oxygenated state (40).

As mentioned above, deoxyHb-trout IV is in the quaternary T state with its subunits in the t state independent of pH. Each of the subunits carries two Bohr groups. For the deoxygenated α subunits, the pK values derived from the binding isotherms are $\mathrm{p}K_{\alpha 1} = \mathrm{p}K_{\alpha 2} = 8.5$ and correspondingly for the β subunits $\mathrm{p}K_{\beta 1} = 7.4$ and $\mathrm{p}K_{\beta 2} = 7.5$ (39). Since no changes of quaternary–tertiary or tertiary–tertiary interaction occur on variation of pH (39), each subunit can be regarded as isolated from the others with respect to the conformational changes caused by the protonation of one of the above Bohr groups. For this reason, deoxyHb-trout IV is a suitable system to study the heme–protein coupling mechanism involved in possible direct interactions between Bohr groups and heme within the same subunit.

Recently, Bosenbeck et al. (41) have measured the band shape of the Raman line resulting from the Fe—N_ϵ (His F8) stretching mode in deoxyHb-trout IV as a function of pH. They found that this band changes its line shape with its peak position shifting from $\nu = 217$ cm^{-1} at pH = 6.1 to 223 cm^{-1} at pH = 8.0. Such shifts seen earlier by many authors (42) have been attributed to changes from the T structure to the more relaxed R structure. Thus, a contradiction arises, because it has been shown from the thermodynamic analysis of the O_2- and CO-binding curves that the molecule remains in its quaternary T and tertiary t structure irrespective of pH (39). This has been resolved by analysis of the line shape of the ν_{Fe-His} Raman line, which could be decomposed into five sublines at 202, 211, 217, 223, and 228 cm^{-1}. The frequencies of these sublines remain fixed on variation of pH. Their intensities, however, show significant changes. The latter could be explained by assuming that each subline is a superposition of sub-sublines, with identical frequencies but different Raman scattering intensities, due to different protonation states of the subunits. By using a titration model to calculate the molar fractions of the four different protonation states within the α and β subunits, all the intensities of the sublines in their dependence on pH could be fitted with the pK values introduced above. It turned out that the lines at 202 and 211 cm^{-1} showed variations of intensities governed by pK values of 8.4/8.5 and could therefore be assigned to the α subunits, whereas pK values of 7.4/7.5 resulted from the intensity variations of the sublines at 223 and 227 cm^{-1}, relating these lines to the β subunits. These results were interpreted by use of a model proposed by Bangcharoenpaurpong et al. (43) and recently modified by Friedman et al. (44), which describes the coupling between the σ^* bond of Fe^{2+} — N_ϵ and the π^* orbitals of the pyrrole nitrogen atoms in terms of the polar angle Θ of the Fe—N_ϵ bond with respect to the normal of the heme-plane and the azimuthal angle φ between the N(I)—Fe—N(III) direction in the heme-plane and the projection of the Fe—N_ϵ direction onto this plane. In this picture the sublines are due to conformations with different values of the polar angle Θ, and the sub-sublines are due to conformations at a given Θ but with different values of the azimuthal angle φ (Fig. 1) due to conformational changes on titration of the Bohr groups. The frequency of the subline is mainly determined by the polar angle, whereas a decrease in the azimuthal angle enhances the intensities of the corresponding lines. Although the ν_{Fe-His} band of HbA also has been found to be composed of different sublines, their intensities remain pH independent between 6 and 9 at low Cl^--concentrations, in accordance with the results obtained from earlier RDS studies (24).

Thus, a considerable heterogenity is present in the heme–protein linkage in Hb-trout IV, which is influenced by proton binding to Bohr groups. This clearly suggests that in contrast to HbA the latter is also directly coupled to the binding sites in the deoxygenated t state. Now the question arises as to how this affects the structure of the prosthetic heme groups. To address this point, we measured the depolarization ratio dispersion of the ν_4 and ν_{10} mode of deoxyHb-trout IV as a function of pH. They can be shown to monitor structural changes of the heme group due to protonation of the above Bohr groups. Our results detail the role of the Fe—His F8 linkage in this direct type of allosteric interaction.

THEORETICAL BACKGROUND

Derivation of the polarizibility tensor

To describe the experimentally obtained REPs and DPDs, it is necessary to extend the theory of Peticolas et al. (20), which is based on Loudon's formalism (45) into fifth order. This accounts for the vibrational sidebands of the B and Q bands by considering the creation and subsequent annihilation of vibrations giving rise to absorption in these bands. Symmetry perturbations from D_{4h} are introduced into this formalism by expanding the vibronic coupling operator in the Hamiltonian with respect to equivalent normal distortions δQ_j^Γ. This leads to the expression

$$\frac{\partial H}{\partial Q_{per}^{\Gamma,R}} = \frac{\partial H}{\partial Q^{\Gamma_R}}\bigg|_{\delta Q=0} + \sum_{\Gamma_j} \frac{\partial^2 H}{\partial Q^{\Gamma_R}\partial Q^{\Gamma_j}}\bigg|_{\delta Q=0} \cdot \delta Q^{\Gamma_j}, \quad (1a)$$

$$\frac{\partial H}{\partial Q_{per}^{\Gamma,\mu}} = \frac{\partial H}{\partial Q^{\Gamma_\mu}}\bigg|_{\delta Q=0} + \sum_{\Gamma_j} \frac{\partial^2 H}{\partial Q^{\Gamma_\mu}\partial Q^{\Gamma_j}}\bigg|_{\delta Q=0} \cdot \delta Q^{\Gamma_j}. \quad (1b)$$

δQ_R^Γ and δQ_μ^Γ relate to the normal coordinate of a Raman vibration and the second vibrational quantum, respectively. δQ_j^Γ represents normal distortions of symmetry type Γ_j, which can be written as

$$\delta Q^{\Gamma_j} = \sum_i \delta Q_i^{\Gamma_j}, \quad (2)$$

where δQ_j^Γ represents distortions proportional to the amplitudes of various different normal coordinates of the symmetry type $\Gamma_j = A_{1g}$, B_{1g}, A_{2g}, and B_{2g}. Introducing this into the fifth-order expansion of the Raman tensor yields the perturbed tensor as

$$\begin{aligned}\beta_{\rho\sigma} = &\sum_{e,s=Q,B}\left[\mu_\rho^{ge}\mu_\sigma^{sg}\left(\sum_\Gamma c_{es}^{\Gamma,R}\hat{T}^\Gamma\right)\tilde{F}_{es}\right] \\ &+ \sum_{e,s,t,u=Q,B}\left\{\mu_\rho^{ge}\mu_\sigma^{\mu g}\times\left\{\left(\sum_\Gamma c_{es}^{\Gamma,R}\hat{T}^\Gamma\right)\right.\right. \\ &\times\left(\sum_\Gamma c_{st}^{\Gamma,\mu}\hat{T}^\Gamma\right)\cdot\left(\sum_\Gamma c_{tu}^{\Gamma,\mu}\hat{T}^\Gamma\right)F_1 \\ &+\left(\sum_\Gamma c_{es}^{\Gamma,\mu}\hat{T}^\Gamma\right)\left(\sum_\Gamma c_{st}^{\Gamma,R}\hat{T}^\Gamma\right) \\ &\times\left(\sum_\Gamma c_{tu}^{\Gamma,\mu}\hat{T}^\Gamma\right)F_2+\left(\sum_\Gamma c_{es}^{\Gamma,\mu}\hat{T}^\Gamma\right) \\ &\left.\left.\times\left(\sum_\Gamma c_{st}^{\Gamma,\mu}\hat{T}^\Gamma\right)\left(\sum_\Gamma c_{tu}^{\Gamma,R}\hat{T}^\Gamma\right)F_3\right\}, \quad (3)\end{aligned}$$

where μ_p^{ge}, μ_σ^{sg} are dipole transition matrix elements connecting the electronic ground state and the excited elec-

tronic states $|e\rangle, |s\rangle$. (ρ, σ = x, y, z label the polarization state of the transition).

The frequency functions F, F_1, F_2, and F_3 are defined by

$$\begin{aligned}
\tilde{F} &= \{(\tilde{\nu}_e + \Omega_R - \tilde{\nu}_L + i\gamma^e)c\tilde{\nu}_s - \tilde{\nu}_L + i\gamma^s)\}^{-1},\\
F_1 &= \{(\tilde{\nu}_e + \Omega_R - \tilde{\nu}_L + i\gamma^e)(\tilde{\nu}_s - \tilde{\nu}_L + i\gamma^s)\\
&\quad \times (\tilde{\nu}_t + \Omega_\mu - \tilde{\nu}_L + i\gamma^t)(\tilde{\nu}_u - \tilde{\nu}_L + i\gamma^u)\}^{-1},\\
F_2 &= \{(\tilde{\nu}_e + \Omega_R - \tilde{\nu}_L + i\gamma^e)(\tilde{\nu}_s + \Omega_R + \Omega_\mu - \tilde{\nu}_L + i\gamma^s)\\
&\quad \times (\tilde{\nu}_t + \Omega_\mu - \tilde{\nu}_L + i\gamma^t)(\tilde{\nu}_u - \tilde{\nu}_L + i\gamma^u)\}^{-1},\\
F_3 &= \{(\tilde{\nu}_e + \Omega_R - \tilde{\nu}_L + i\gamma^e)(\tilde{\nu}_s + \Omega_R + \Omega_\mu - \tilde{\nu}_L + i\gamma^s)\\
&\quad \times (\tilde{\nu}_t + \Omega_R - \tilde{\nu}_L + i\gamma^t)(\tilde{\nu}_u - \tilde{\nu}_L + i\gamma^u)\}^{-1}. \qquad (4)
\end{aligned}$$

Antiresonant terms have been omitted for simplicity; ν_e, ν_s, ν_t, ν_u are the wavenumbers of the electronic transitions from the groundstate $|g\rangle$ into $|e\rangle$, $|s\rangle$, $|t\rangle$, and $|u\rangle$ excited electronic states, which are indicating Gouterman's unmixed Q and B states of the porphyrin system (46), respectively. γ^e, γ^s, γ^t, and γ^u label the corresponding halfwidths, ν_L is the frequency of the incident laser light, $\Omega_R(\Omega_\mu)$ is the frequency of the Raman mode (the second vibration). The constants $c_{e,s}^{\Gamma,R}$, $c_{e,s}^{\Gamma,\mu}$ are related to the following matrix elements of the vibronic coupling operators described by Eqs. 1a and 1b:

$$\begin{aligned}
c_{e,s}^{\Gamma,R} &= \left\langle e\left|\frac{\partial H}{\partial Q^{\Gamma_R}}\right|_{\delta Q=0} + \frac{\partial^2 H}{\partial Q^{\Gamma_R}\partial Q^{\Gamma_j}}\right|_{\delta Q=0}\cdot \delta Q^{\Gamma_j}\left|s\right\rangle Q_R^{01},\\
c_{e,s}^{\Gamma,\mu} &= \left\langle e\left|\frac{\partial H}{\partial Q^{\Gamma_\mu}}\right|_{\delta Q=0} + \frac{\partial^2 H}{\partial Q^{\Gamma_\mu}\partial Q^{\Gamma_j}}\right|_{\delta Q=0}\cdot \delta Q^{\Gamma_j}\left|s\right\rangle Q_\mu^{01}. \qquad (5)
\end{aligned}$$

$Q_R^{01} = \langle 1|Q^{\Gamma_R}|0\rangle$ and Q_μ^{01} label the vibrational matrix elements. $\Gamma_R(\Gamma_\mu)$ are the representations of the Raman mode (second vibration) and Γ_j that for the normal distortion δQ^{Γ_j}. Γ labels the product representations $\Gamma_R \times \Gamma_j$ and $\Gamma_\mu \times \Gamma_j$ for each Γ_j.

It should be noted that the above matrix elements are related to the distortion of the equilibrium configuration of the excited electronic states $|e\rangle$ and $|s\rangle$ with respect to the electronic ground state along the normal distortions δQ^{Γ_j}. Consequently, variations in c_{es}^{Γ} may reflect configurational changes in both the ground state and the excited electronic states involved (47). The vibronic coupling parameters can be classified as follows:

(*a*) $c_{QQ}^{A_{1g}}$ and $c_{BB}^{A_{1g}}$ reflect intrastate Frank–Condon (FC) coupling in the Q and B state,

(*b*) c_{QB}^{Γ} ($\Gamma = A_{1g}, B_{1g}, B_{2g}, A_{2g}$) describes interstate Herzberg–Teller coupling between Q and B, and

(*c*) c_{QQ}^{Γ} and c_{BB}^{Γ} ($\Gamma = B_{1g}, B_{2g}$) are related to intrastate Jahn–Teller coupling within Q and B.

Using the above expression for $\beta_{\rho\sigma}$ and Placzek's (48) formalism for calculating REP and DPD of distinct Raman lines from their tensor components, we are able to fit the theory to the experimental data of the polarized REPs with one common set of fit parameters $c_{e,s}^{\Gamma,R}$ and $c_{e,s}^{\Gamma,\mu}$ (e, s = Q, B; $\Gamma = A_{1g}, B_{1g}, A_{2g}$, and B_{2g}). These parameters $c_{e,s}^{\Gamma,R}$, $c_{e,s}^{\Gamma,\mu}$ are in first order linearly related to the perturbations δQ^{Γ_j}. Thus, they contain information about possible asymmetric heme–protein interactions.

It should be mentioned that in case of strict D_{4h} symmetry, the depolarization ratio is $\rho = 0.125$ for A_{1g} lines, $\rho = 0.75$ for B_{1g} and B_{2g} lines, and $\rho = \infty$ for A_{2g} lines independent of the excitation wavelengths (49). Symmetry-lowering distortions δQ^{Γ} introduce dispersion of the depolarization ratio, which by this mechanism is an ideal tool to detect interactions between the heme group and the protein inducing such distortions.

So far the theory considers only one conformational type of Hb molecules to be present. In reality, due to various subunit heterogenity protonation processes and conformational transitions, many conformational states of the molecules with different polarizibility tensors are simultaneously present in the solution. The total scattering intensity is therefore an incoherent superposition of the intensities of these differing species of molecules. Therefore, as has been shown elsewhere (20), each tensor element of the effective Raman tensor can be expressed by:

$$|\beta_{\rho\sigma}^{\text{eff}}| = \left\{\sum_l X_l(\beta_{\rho\sigma})_l^2\right\}^{1/2}, \qquad (6)$$

where X_l denotes the mole fraction of the lth conformation, the corresponding Raman tensor is denoted by $(\beta_{\mu\sigma})_l$. Some straightforward but lengthy calculations lead to the following expression for the effective distortion parameters, which are the result of a fitting procedure of the theoretical expression to the observed REPs and DPD (20).

$$|c_{e,s}^{\Gamma}(\text{pH})| = \left\{\sum_l X_l(c_{e,s}^{\Gamma})_l^2\right\}^{1/2}, \qquad (7)$$

$(c_{e,s}^{\Gamma})_l$ are the vibronic coupling parameters of the Raman fundamental related to the lth conformation.

MATERIALS AND METHODS

Preparation of Hb-trout IV

The blood for the preparation was obtained from commercially purchased trout salmo iredius. It was washed several times with 0.9% aqueous solution of NaCl containing ethylenediaminetetraacetate to avoid coagulations and afterward hemolized with distilled water. The obtained Hb solution was then dialyzed against 0.1 M tris(hydroxymethyl)-aminomethane (Tris)-HCl buffer at pH 9.1. After equilibration it was applied to a DEAE-Sephadex A50-column from Sigma Chemical Co. (St. Louis, MO) (dimension 40 × 2 cm). The pH gradient elution was carried out using two containers, one with 0.1 M Tris-HCl buffer at pH 9.1 and the other with 0.1 M KH_2PO_4 at pH 4.5. The different pH values were adjusted dialyzing against 0.1 M Tris-HCl buffer (pH > 7.0) and 0.1 M bis-Tris-HCl buffer (pH < 7.0). The samples were deoxygenated by adding a few grains of $Na_2S_2O_4$ and were thermostated at 4 ± 0.5°C. The concentration of each sample was 1.0×10^{-3} M and monitored by measuring the optical absorbance with an HP-diode array spectrometer.

Experimental arrangement

The exciting radiation was obtained using an argon ion laser from Spectra Physics (Darmstadt, Germany). The laser beam was polarized

perpendicularly to the scattering plane and focused by a cylindrical lens onto a sample. The Raman radiation was measured in backscattering geometry. A polarization analyzer between sample and spectrometer enabled us to measure the intensity of the two components perpendicular and parallel to the scattering plane. A polarization scrambler was used to avoid different transmissions of the spectrometer for different polarization. The Raman radiation was analyzed with a Czerny–Turner double monochromator (Spex, Munich, Germany) collected by a photocounting system (Ortec, Munich, Germany) and digitized by a microcomputer, where it was stored for further analysis. To calculate the correct height of the Raman lines, a program was used to subtract fluorescence background and to decompose complex spectra into distinct Lorentzian lines of defined widths and heights. The intensities of the Raman lines were compared with the intensity of the SO_4^{2-} line at 980 cm^{-1} in a separate sample containing $(NH_4)_2SO_4$ and 1 mM deoxyHb. By this method, the SO_4^{2-} line was used as internal standard for correction of the Raman intensities with respect to laser power and transmission of the spectrometer. Since at the given concentration of deoxyHb corrections for absorption are not necessary (35), we did not correct the intensities of the SO_4^{2-} line and of the Hb lines for different absorption due to their differing wavelengths of the Raman light. Depolarization ratios of the Raman lines were measured in the absorption of the Q band by using an excimer laser (EMG MSC; Lambda Physics, Göttingen, Germany) and pumped dye laser (model FL 2001; Lambda Physics) with a conventional Raman spectrometer (1877 Triple Mate; Spex) and a diode array camera (O-SMA; Spectroscopy Instruments) for detection of the signal. Details are given by Bobinger et al. (50).

Fitting procedure

A program called MINUITL from the CERN library (Computer Center, University of Bremen) was used in a least-squares fit to the experimental DPDs and REPs. In a first approximation, all fits were carried out in the framework of Gouterman's four-orbital model, which imposes the following restrictions on the vibronic coupling parameters (49):

$$c_{QQ}^{B1g} = -c_{BB}^{B1g}; \quad c_{QQ}^{B2g} = -c_{BB}^{B2g}. \tag{8}$$

In most cases a satisfactory fit could not be obtained under these restrictions. Consequently, they have been relaxed, and c_{QQ}^{Γ} and c_{BB}^{Γ} ($\Gamma = B_{1g}$, B_{2g}) were used as free parameters. The quality of the fits was judged by means of the error value calculated by f, which is a function of the fit parameters

$$f = \{\sum \chi_i^2/(N\sigma_i^2)\}^{1/2}, \tag{9}$$

where χ_i^2 is the χ^2 value of the ith data point with respect to the fit and σ_i is its statistical error. N denotes the number of data points. The best fit is selected by the minimum of f in dependence on the fitting parameters. To estimate the statistical errors of the vibronic coupling parameters, we calculated the normalized error value f/f_{min} as a function of the distinct parameters c_{es}^{Γ} in the vicinity of the respective minimum of the χ^2 function. It turned out that inappropriate fits are obtained for f/f_{min} larger than 1.02. Thus, we considered $\delta c_{es}^{\Gamma} = \pm c_{es}^{\Gamma}(f_{min}) - c_{es}^{\Gamma}(1.02 \cdot f_{min})|$ as the statistical error of the vibronic coupling parameter c_{es}^{Γ}.

Since B_{1g}- and B_{2g}-type contributions to the polarizability tensor cannot be discriminated by polarization experiments on randomly oriented molecules, we omitted all c_{es}^{B2g} parameters in the fit to the data. Thus, the vibronic coupling parameters c_{es}^{B1g} may also reflect some minor contributions from B_{2g}-type coupling to the scattering tensor. B_{1g}-type coupling, however, can be expected to be predominant for both lines investigated, because the ν_{10} mode exhibits B_{1g} symmetry in D_{4h}, and the N_P atoms mainly involved in the heme–protein interaction affecting the ν_4 mode cannot contribute to B_{2g}-type coupling. To express the coupling parameters c_{es}^{Γ} in absolute units (cm^{-1}), we considered explicitly their contribution to the fifth-order term of the polarizability tensor as described in detail by Schweitzer-Stenner et al. (51) and Bobinger et al. (52). The remaining multimode contributions to the fifth-order term are represented by an effective helping vibration (51).

Our experimental data sets cover the region between 22,000 and 18,900 cm^{-1}. The vibronic coupling parameters determine these DPDs and REPs to a different extent. For the ν_4 mode, c_{QB}^{Γ} and c_{BB}^{Γ} provide larger contributions to its Raman cross-section than c_{QQ}^{Γ}. In contrast, c_{QQ}^{Γ} and c_{QB}^{Γ} mainly determine the cross-section of ν_{10}, for which c_{BB}^{Γ} is of minor importance. As a consequence, statistical errors of the c_{BB}^{Γ} (ν_{10}) and c_{QQ}^{Γ} (ν_4) values are larger than those of the remaining parameters. The accuracy to which the c_{es}^{Γ} can be determined is demonstrated by earlier Raman dispersion studies on oxyHb-BME (26, 28). Since the Bohr effect is absent in this modified Hb, the DPDs and REPs of ν_4 and ν_{10} exhibit only small variations in dependence of pH, which are within the experimental errors. The corresponding c_{es}^{Γ} also show only slight changes with pH (26).

RESULTS

Depolarization dispersion of the ν_4 mode

We have measured the polarized REPs of the ν_4 line of the porphyrin macrocycle at 1,355 cm^{-1}. The line results from an A_{1g} normal vibration determined by a half pyrrole stretching vibration consisting of out-of-phase motions of N—C_α and C_α—C_β bonds (53). Its dispersion of the DPD mainly probes distortions of the pyrrole nitrogens and the C_α carbons caused by their interaction with the Fe^{2+} ligands (20, 54). This is due to the large amplitudes of the involved N—C_α stretching vibrations. Since by group theory the symmetry Γ of the vibronic coupling matrix elements c_{es}^{Γ} is related to the representation Γ_R of the Raman mode and the representation Γ_j of the distortion δQ^{Γ_j} by $\Gamma = \Gamma_R \times \Gamma_j$, c_{es}^{A1g} elements reflect distortions of A_{1g} symmetry. Consequently, the matrix elements c_{es}^{B1g} and c_{es}^{A2g} result from symmetry-lowering distortions of B_{1g} and A_{2g} type, respectively.

As shown in a recent article (54), the above B_{1g} and A_{2g} distortions can be related to the geometry of the heme-Im F8 complex (shown in Fig. 1) by means of the following coupling model. If the imidazole eclipses the line N(I)—Fe^{2+}–N(III) (azimuthal angle $\varphi = 0$), B_{1g}-type distortions are induced by repulsive interactions between N(I), N(III) of the porphyrin, and C_ϵ, C_δ of Im F8 (3, 21), respectively. They increase with increasing tilt angle Θ and decreasing Fe displacement δ. If the azimuthal angle of the proximal imidazole increases, A_{2g}- and B_{2g}-type distortions are induced by perturbations of the α carbons, whereas the B_{1g} distortions decrease, owing to the reduced perturbations of the pyrrole nitrogens. At a fixed azimuthal angle Φ, the magnitude of A_{2g} and B_{2g} distortions depends on the tilt angle Θ and the Fe displacement δ. This model is refered to as heme-ligand coupling (HLC) model.

The fits to the DPDs and REPs were performed using the vibronic coupling matrix elements c_{es}^{Γ} as free parameters. To express them in absolute units, we considered explicitly their contribution to the fifth-order term of the polarizability tensor and the vibronic side band Q_v of the optical absorption spectrum as described in detail by

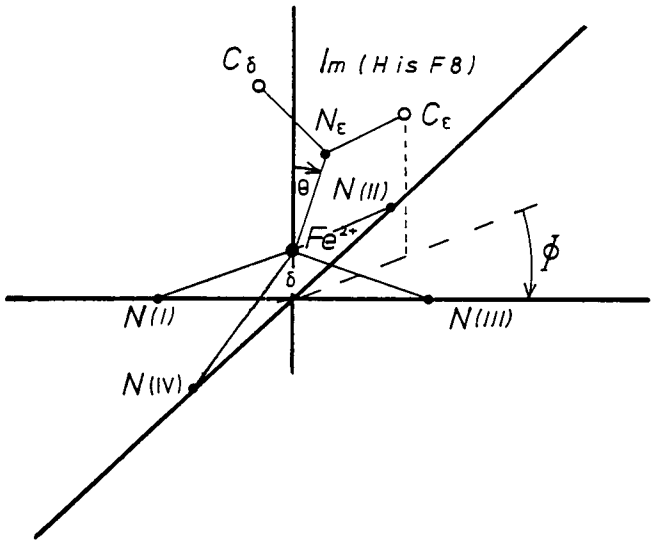

FIGURE 1 Schematic representation of the heme-N_ϵ(His F8) complex. N(I), N(II), N(III), and N(IV) are the pyrrole nitrogens, Θ is the tilt angle of the Fe^{2+} — N_ϵ(His F8) bond with respect to the heme normal, and Φ is the azimuthal angle formed by the line N(I) — Fe — N(III) and the projection of the imidazole of the heme.

Schweitzer-Stenner et al. (51). Electronic distortions have not been considered explicitly because their determination requires REPs and DPD data covering the Q_0-band region (54). To derive the correct energy positions and the corresponding transition dipole moments of the Q and B band (cf. Eq. 3), the latter were deconvoluted into two Lorentzians according to the Q_0 and Q_v bands and the B_0 and B_v bands, respectively. By integrating over the Lorentzians of the Q_0 and B_0 bands, the respective dipole transition moments were derived. The parameters thus obtained are $E_{Q_0} = 17{,}035\ cm^{-1}$, $E_{B_0} = 23{,}042\ cm^{-1}$, $\mu^{gQ} = 1.23$ Debye, and $\mu^{gB} = 7.26$ Debye (55). These values have been used as fixed parameters in our fit to the data.

The use of Lorentzian profiles for the analysis of the optical bands requires some further comments. It is well known from several studies on optical spectra of deoxygenated heme proteins that at least their B bands are subject to inhomogeneous broadening (56–58). Hence, an exact fit to their band shape required either a deconvolution into two or more Gaussian subbands or the application of an asymmetric distribution function (56). In our case, however, we only need a good estimation of the ratio μ^{gQ}/μ^{gB} to obtain a consistent set of c^{Γ}_{es} (54). For this purpose, Lorentzian fits to the absorption bands provide sufficient information.

Three data sets consisting of polarized REPs and DPDs measured at pH 6.4, 7.2, and 8.1 are displayed in Fig. 2. The solid lines were obtained by using the theoretical expressions for the DPD and REPs derived from the polarizability tensor in Eq. 3 in the fits to the data. Owing to the low energy of Q_0 state, the data points observed by an argon ion laser cover only the preresonant region of the Q_v and B_0 band, in contrast to the situation in oxyHb-trout IV, where Q_v-resonance enhancement can be probed using an excitation wavelength of 528 nm (40). One may therefore doubt whether fits to the above DPDs and REPs yield the correct vibronic coupling parameters. To give more evidence for the reliability of our fits, we measured some DPR values between the resonance positions Q_0 and Q_v at the above pH values by using an excimer-pumped dye laser. As shown in Fig. 2, these data points (indicated by arrows) nicely agree with the DPD curves calculated from the fits to the corresponding data observed with the argon ion laser.

Altogether we fitted DPDs and REPs measured at 16 different pH between 6.0 and 9.0. All data sets could be fitted using only c^{Γ}_{es} with $\Gamma = A_{1g}$ and B_{1g}.

The c^{B1g}_{es} are considerably large, especially in the alkaline region. This is reflected by the DPDs that exhibit rather large DPR values at their maxima positioned between the Q_{01}/Q_{10}- and Q_{11} resonance positions (DPR = 0.4–0.5) compared with corresponding values found for deoxyHbA and deoxyMb (DPR = 0.2–0.3) (54). A_{2g}-type contributions are weak and cannot be resolved unambiguously from the experimental data. This clearly suggests that the ν_4 mode is subject to asymmetric B_{1g} perturbations. The pH dependence of the coupling parameters (Raman titration curves [RTC]) is shown in Fig. 3. The full lines herein result from a titration model, which will be discussed below.

Depolarization dispersion of the ν_{10} line

Normal coordinate analysis on Ni(II)-octaethylporphyrin has shown that the structurally sensitive ν_{10} mode (B_{1g} in D_{4h}) results from C_m — C_α stretching vibrations, C_m — H bending, and C_β vibrations along the C_β — PS bonds. The latter provide only small contributions to the potential energy distribution of the mode but this does not imply that its contribution to vibronic coupling is small. The pyrrole nitrogens do not show any significant displacements (53). As a consequence one expects that the DPD of the ν_{10} line mainly probes peripherical coupling between the macrocycle (i.e., the pyrrole carbons) and the corresponding PS. This can be modulated by noncovalent interactions between the PS and amino acid residues in the heme cavity (20). As shown in our recent article (30), the PS can be expected to cause symmetry-lowering distortions of B_{2g} and A_{2g} symmetry, provided that identical PS are sterically equivalent. This gives rise to vibronic coupling parameters c^{Γ}_{es} with $\Gamma = A_{2g}$ (for B_{2g} distortions) and B_{2g} (for A_{2g} distortions). Asymmetric B_{1g} distortions are only imposed if identical but sterically inequivalent PS cause different perturbations of the corresponding pyrroles. The symmetry of the thus induced c^{Γ}_{es} is A_{1g}. Fig. 4 depicts DPDs and REPs of the ν_{10} mode measured at pH 6.4, 7.2, and 8.1. The full lines result from fits to the data obtained with an argon

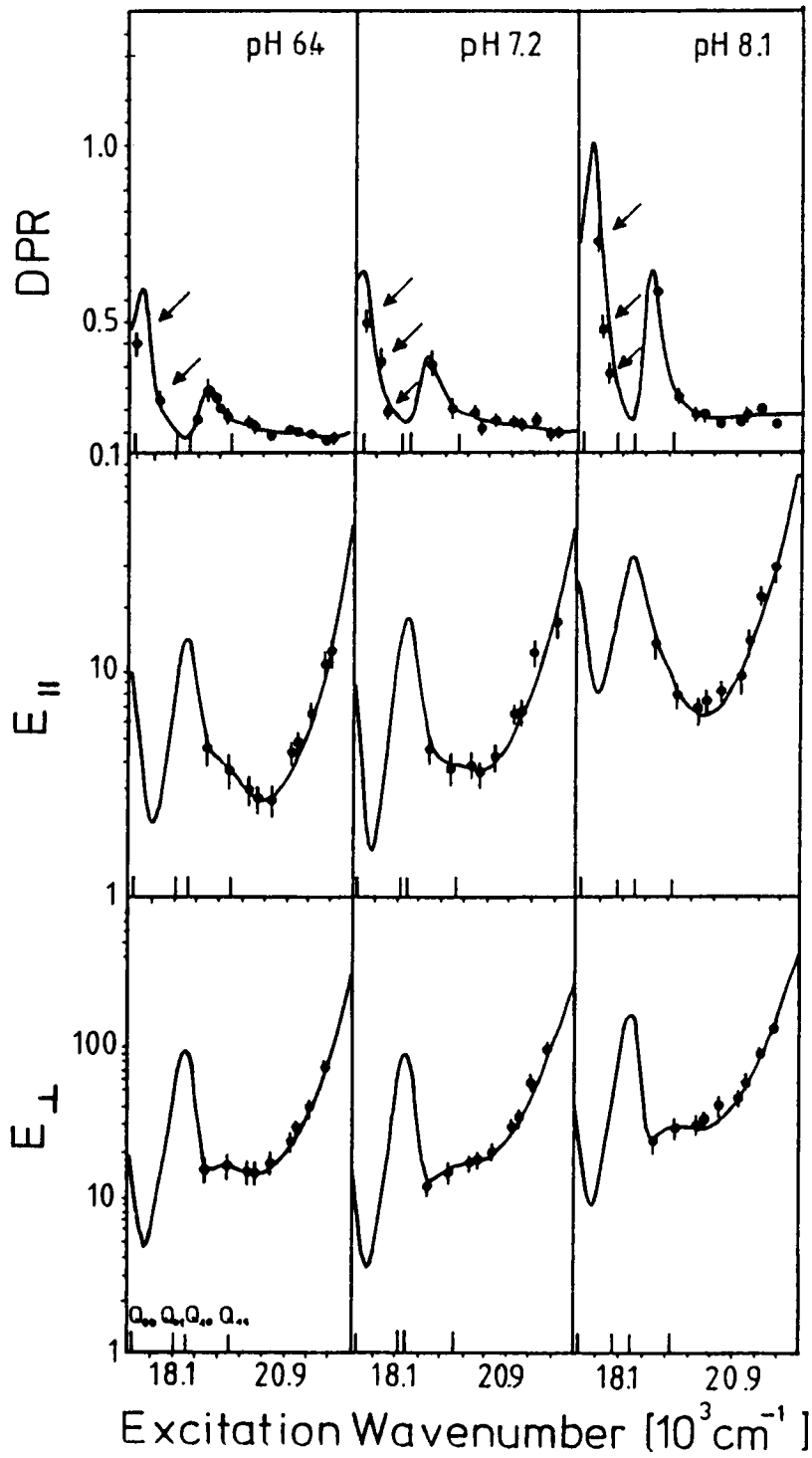

FIGURE 2 DPDs and polarized REPs of the ν_4 line (1,355 cm^{-1}) of deoxyHb-trout IV measured at pH 6.4, 7.2, and 8.1. The solid lines result from a fit to the data. The arrows label the data points measured by means of an excimer pumped dye laser. The resonance positions Q_{01}, Q_{10}, and Q_{11} are marked in the DPD diagrams.

ion laser. They give again a good prediction to the DPR values in the region between the Q_{00} and Q_{11} resonance positions as shown by the corresponding DPR values indicated by arrows.

Only coupling parameters of A_{1g} and B_{1g} symmetry were necessary for the reproduction of the experimental data, suggesting that the ν_{10} mode is affected by B_{1g}- rather than by B_{2g}-type distortions. The c_{es}^{A1g} are in the same order of magnitude as the corresponding c_{es}^{B1g}, indicating that the asymmetric B_{1g} distortions are considerably strong. Fig. 5 displays the RTCs of the c_{es}^{Γ}, which are again derived from DPD and REPs measured at 16 dif-

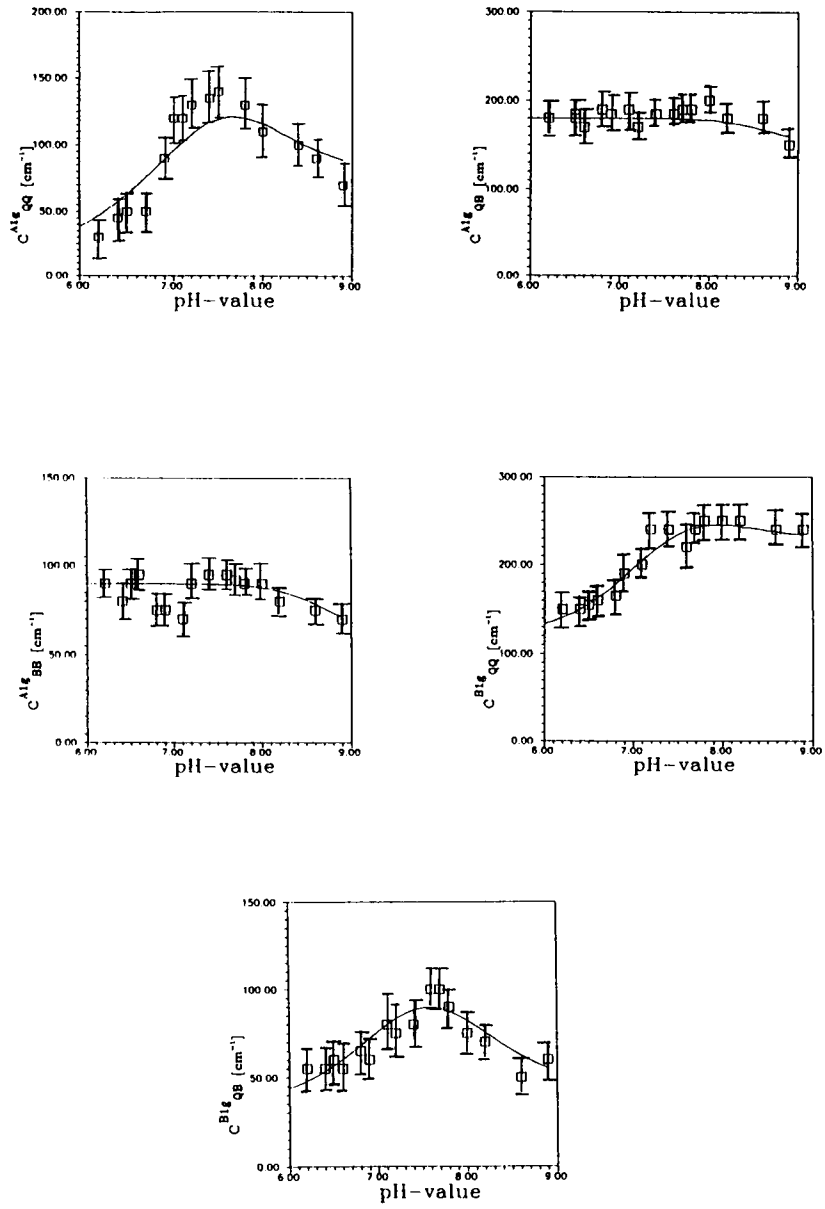

FIGURE 3 RTCs of the effective vibronic coupling parameters c_{es}^{Γ} derived from the fits to the DPDs and REPs of the ν_4 mode of deoxyHb-trout IV. The solid lines result from a fit to a titration model described in the text.

ferent pH. The solid lines in the diagrams result from fits, which will be discussed below.

Analysis of Raman titration curves

To rationalize the pH dependence of the effective distortion parameters, we consider the titration states of the α and β subunits, which can be regarded as jointly independent. From Eq. 7 the pH dependence of the coupling parameters is related to the molar fractions $X_u(i,j)$ of the titration states in α and β subunits with $pK_{1\alpha} = pK_{2\alpha} = 8.5$ and $pK_{1\beta} = 7.4$, $pK_{2\beta} = 7.5$, respectively. (i, j) denote the occupation of the titratable sites with protons (i, j = 0, 1) and u denotes the subunit α or β. Therefore, one expects variations of the c_{es}^{Γ} in the region of pH $\approx$ 7.5 and also pH $\approx$ 8.5. Inspection of the RTCs of the ν_4 mode in Fig. 3, however, shows that the parameters c_{QQ}^{A1g}, c_{QQ}^{B1g}, c_{QB}^{B1g} show strong variations with a maximum or an inflection point at pH 7.5, whereas the parameters c_{QB}^{A1g} and c_{QB}^{A1g} show no variations in this region. Instead, a slight decrease of their values is observed for pH > 8.3.

All RTCs of the ν_{10} mode exhibit the strongest variations in the region at 7.5. From this we try the following reasoning. For c_{QQ}^{A1g}, c_{QQ}^{B1g}, and c_{QB}^{B1g}, we assume that their RTCs mainly reflect a dependence of the corresponding vibronic coupling parameters $c_{es}^{\Gamma}(i,j)_{\beta}$ on the titration state $(i,j)_{\beta}$ in the β subunits. For reasons of simplicity, we further assume that for the two α chains, the corresponding $c_{es}^{\Gamma}(i,j)_{\alpha} = c_{es,\alpha}^{\Gamma}$ are identical, i.e., independent

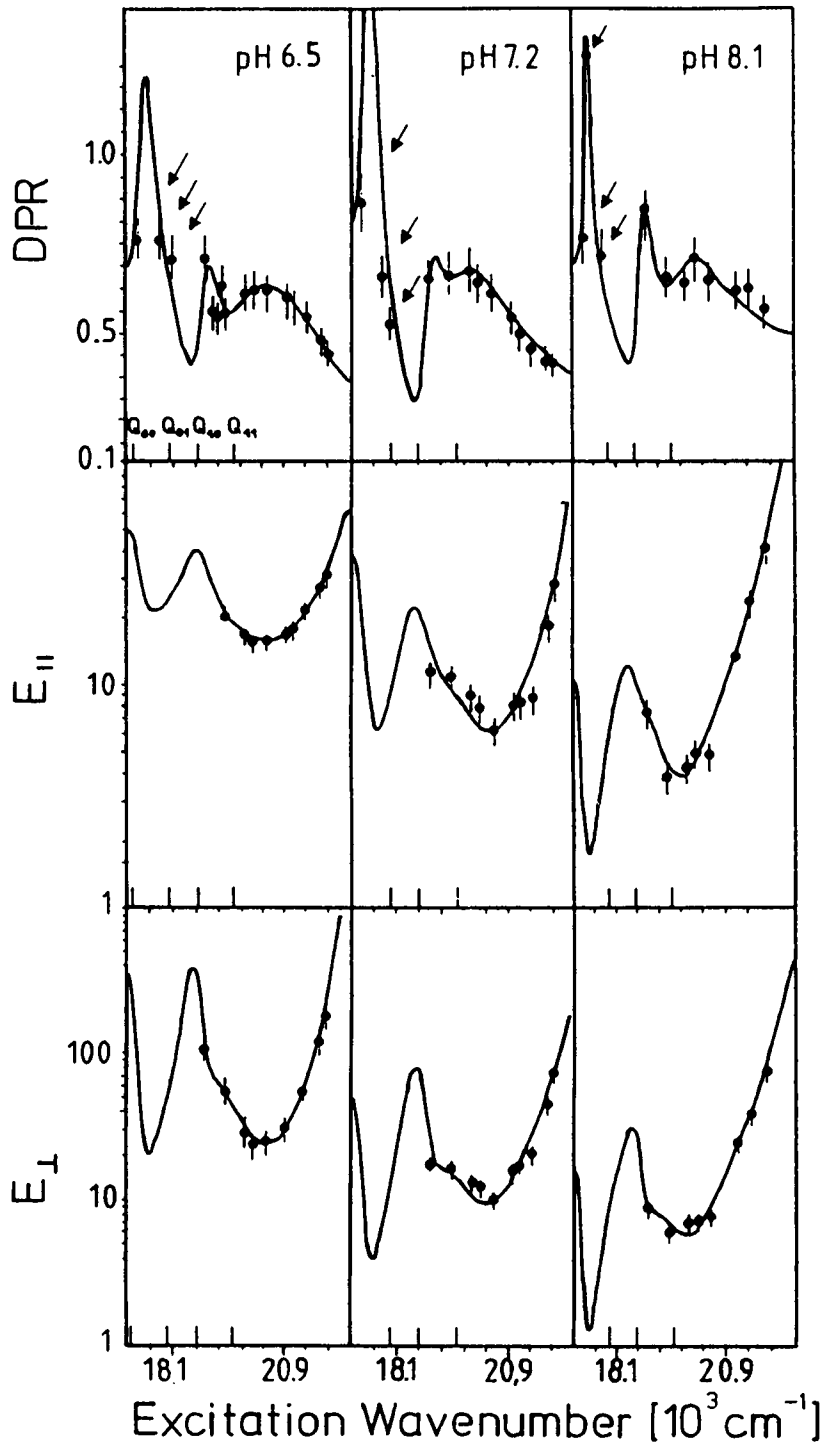

FIGURE 4 DPDs and polarized REPs of the ν_{10} line (1,607 cm^{-1}) of deoxyHb-trout IV measured at pH 6.4, 7.2, and 8.1. The solid lines result from a fit to the data. The arrows label the data points measured by means of an excimer dye laser. The resonance positions Q_{01}, Q_{10}, and Q_{11} are marked in the DPD diagrams.

of the titration state $(i, j)_\alpha$, even though we cannot exclude that they are slightly different. In this case, by simple algebra from Eq. (7) one finds

$$(c_{es}^{\Gamma})_\beta^2 = \sum_{i,j} X_\beta(i, j)[(c_{es}^{\Gamma}(i, j)_\beta)^2 + (c_{es,\alpha}^{\Gamma})^2] = \sum_{i,j} X_\beta(i, j)c_{es}^{\Gamma}(i, j)^2. \quad (10)$$

A corresponding expression is obtained by interchanging α and β, in the case that the α subunits exhibit $c_{es}^{\Gamma}(i, j)_\alpha$, which are dependent on their titration states, whereas the parameters of the β chains are constant. This has been assumed to be approximately valid for c_{QB}^{A1g} and c_{BB}^{A1g} of the ν_4 mode. Based on the above approximations, Eq. 7a has been used to fit the pH dependence of the effective

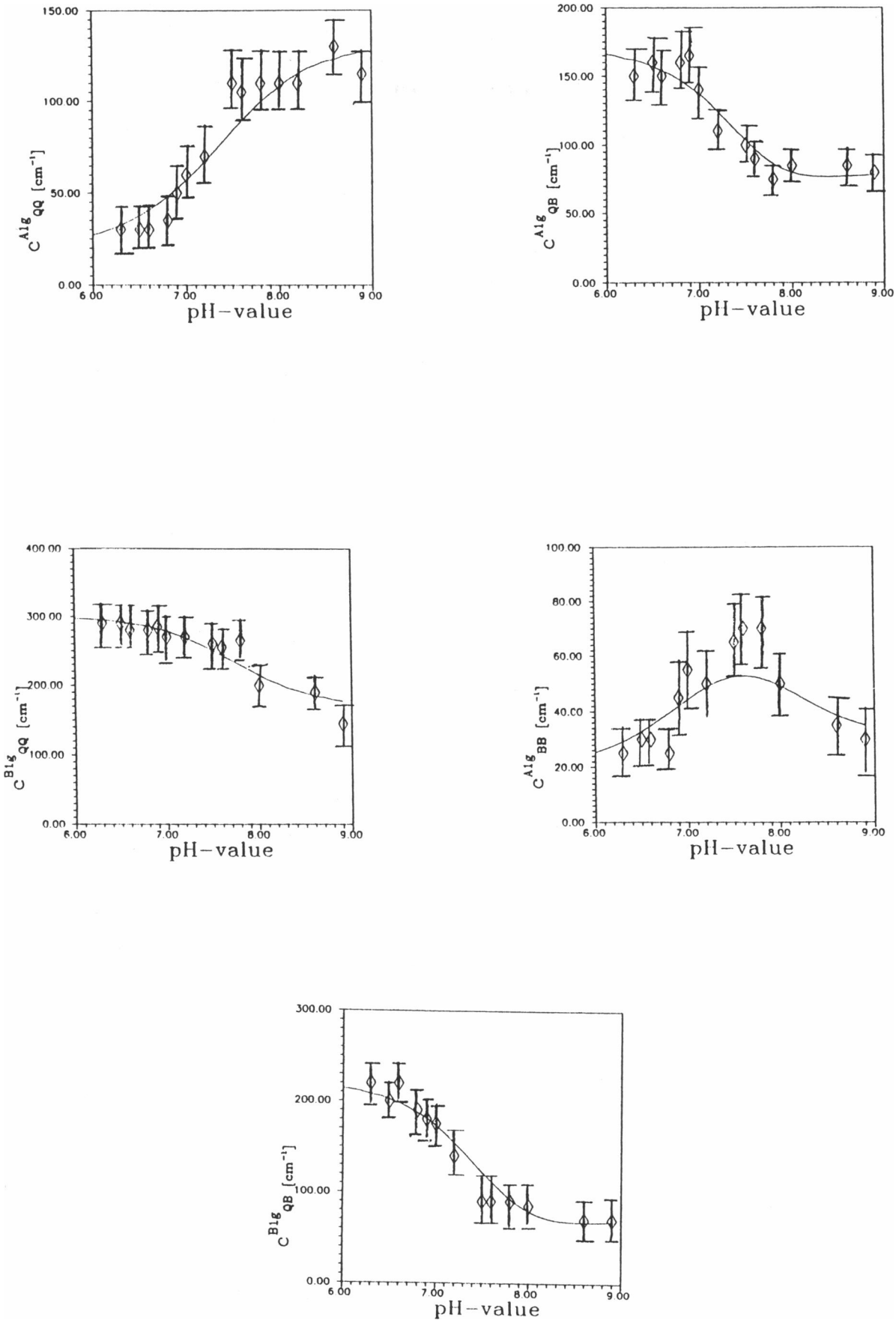

FIGURE 5 RTCs of the effective vibronic coupling parameters of c^{Γ}_{es} derived from the fits to the DPDs and REPs of the ν_{10} mode of deoxyHb-trout IV. The solid lines result from a fit to a titration model described in the text.

coupling parameters of the ν_4 (Fig. 3) and the ν_{10} line (Fig. 5). This was done by using the $c^{\Gamma}_{es}(i,j)_u$ as fit parameters. These parameters are listed in Table 1 and 2 for the ν_4 and ν_{10} line, respectively. It should be noted that due to the almost identical pK values in the α and β chains, respectively, $X_u(0, 1) = X_u(1, 0)$. Therefore, only the sum of c^{Γ}_{es} (0, 1) and c^{Γ}_{es} (1, 0) can be determined. As demonstrated by the solid lines in Fig. 3 and 5, this procedure yields satisfactory fits to the RTCs. Some deviations from the data points for c^{A1g}_{QQ} (ν_4) and c^{A1g}_{BB} (ν_{10}) seem to indicate that in contrast to our assumptions, the corresponding $c^{A1g}_{es,\alpha}$ are not independent of the titration state [i, j]. It should be noted, however, that the corresponding data are subject to larger statistical errors for reasons outlined under Material and Methods.

DISCUSSION

Heme–protein coupling monitored by the DPD of the ν_4 mode

It is known for several Hb derivatives that the ν_4 mode is responsive to conformational changes of the Fe—His F8 linkage. Its frequency exhibits an inverse correlation with that of the ν_{Fe-His} stretching mode (59). This observation can be rationalized by assuming that a larger out of plane displacement δ of the iron increases the population of the anti-bonding $a_1(d_{z^2}\text{-}\sigma_L)$MO of the Fe—Im complex and reduces the $e_g(d_\pi)\text{-}e_g(\pi^*_{porph})$ overlap. Whereas the first effect reduces the ν_{Fe-Im} frequency, the latter one increases the ν_4 frequency (6). As also has been shown for several heme proteins, the DPD of the ν_4 mode is responsive to interactions between C_ϵ and C_δ of the proximal imidazole and the atoms of the heme core, namely the pyrrole nitrogens N(I), N(III), and the adjacent C_α (20, 54). Owing to the HCL model briefly described in the result section (54), this type of heme–protein coupling depends on the parameters δ (Fe^2 displacement), Θ (tilt angle), and Φ (azimuthal angle) of the

TABLE 1 Vibronic coupling parameters $c^{\Gamma}_{es}(i, j)_u$ of the ν_4 mode

	(0, 0)	(0, 1) + (1, 0)	(1, 1)	Subunit
c^{B1g}_{QQ}	230	560	120	β
c^{B1g}_{QB}	45	240	35	β
c^{A1g}_{QQ}	80	120	10	β
I_{223}	70	160	40	β
I_{228}	60	92	25	β
c^{A1g}_{QB}	140	360	180	α
c^{A1g}_{BB}	50	180	90	α
I_{202}	6	20	65	α
I_{211}	15	100	69	α
I_{217}	30	60	80	α

Vibronic coupling parameters $c^{\Gamma}_{es}(i, j)_u$ of the ν_4 mode derived from fitting the titration model described in the text to the RTCs in Fig. 3. The parameters are expressed in units of cm^{-1}. The intensities I (in arbitrary units) of the sub-sublines of the five sublines from the $\nu_{Fe\text{-}His}$ vibration [41] are given for comparison.

TABLE 2 Vibronic coupling parameters $c^{\Gamma}_{es}(i, j)_\beta$ of the ν_{10} mode

	(0, 0)	(0, 1) + (1, 0)	(1, 1)	Subunit
c^{A1g}_{QQ}	130	160	20	β
c^{A1g}_{BB}	20	140	20	β
c^{B1g}_{QQ}	170	500	300	β
c^{A1g}_{QB}	80	100	170	β
c^{B1g}_{QB}	70	80	220	β

Vibronic coupling parameters $c^{\Gamma}_{es}(i, j)_\beta$ of the ν_{10} mode derived from fitting the titration model described in the text to the RTCs in Fig. 5. The parameters are expressed in units of cm^{-1}.

Fe—His F8 complex (cf. Fig. 1). Consequently, one expects some correlation between the pH dependence of the c^{Γ}_{es} (ν_4) and that of vibronic coupling parameters determining the intensity of the ν_{Fe-His} stretching band.

In a recent study from our laboratory (41), we have shown that the profile of the ν_{Fe-His} band can be decomposed into five different sublines. Although their intensities are found to be a function of pH, their frequencies remain unaltered. This was interpreted by use of the coupling model suggested by Friedman et al. (44), which is based on earlier considerations by Bangcharoenpaurpong et al. (43). It relates frequency changes to the variations of the tilt angle Θ, whereas the azimuthal angle Φ was assumed to determine the intensity. The protonation of Bohr groups was assumed to change the azimuthal angle φ and thus the intensities of the sub-subline. The different sublines were related to different tilt angles Θ of the Fe—N$_\epsilon$(His F8) bond.

This interpretation is consistent with the RDS data on the ν_4 mode owing to the following considerations. In view of the HLC model, a decrease in Φ results in larger perturbations of the pyrrole nitrogens N(I) and N(III) that enhance asymmetric B_{1g} distortions of the ν_4 mode. This should be reflected by the vibronic coupling parameters c^{B1g}_{es}, which must be considered as effective ones with respect to the sublines. From Table 1 we read that $c^{B1g}_{es}(1.1) < c^{B1g}_{es}(0.0) < c^{B1g}_{es}(0.1) + c^{B1g}_{es}(1.1)$. As shown above, this reflects different titration states of the β subunit. According to Bosenbeck et al. (41), the intensities $Ic_{i,j}$ of the ν_{Fe-His} sublines at 223 cm^{-1} ($\Omega_{\beta 1}$) and 227 cm^{-1} mainly depend on the protonation of the Bohr groups in the β subunit. From Table 1, one reads that $I(1, 1) < I(0, 0) < I(0, 1) + I(1, 0)$ for both lines. This shows that the pH dependence of the subline intensities parallel that of the c^{B1g}_{es} of the ν_4 mode, in full accordance with what one would expect if both parameters are governed by the azimuthal angle Φ. The heme–imidazole interaction also changes the symmetric coupling parameters c^{A1g}_{es}. While c^{A1g}_{QQ} exhibit a pronounced variation on protonations of the Bohr groups in the β subunit, c^{A1g}_{QB} and c^{A1g}_{BB} show only a slight pH dependence above 8.0, which mainly reflects different titration states of the α subunit. Table 1 shows that $c^{A1g}_{QQ}(1, 1) < c^{A1g}_{QQ}(0, 0) < c^{A1g}_{QQ}(1, 0) + c^{A1g}_{QQ}(0, 1)$, indicating that this parameter also depends on Φ.

For c_{QB}^{A1g} and c_{BB}^{A1g}, one finds a different relation, namely $c_{es}^{A1g}(0,0) < c_{es}^{A1g}(1,1) < c_{es}^{A1g}(0,1) + c_{es}^{A1g}(1,0)$. We compare this with the intensities of the ν_{Fe-His} sublines at 202, 211, and 217 cm^{-1} which are mainly influenced by protonations in the α subunit (41). For each of these sublines, one finds $I(0,0) < I(1,1)$, which again correlates nicely with the corresponding coupling parameters c_{es}^{A1g}. Thus, the comparison of the pH dependence of $c_{es}^{\Gamma}(\nu_4)$ and the intensities of the sub-sublines provide evidence that both are governed by the same structural parameter, which may be identified with the azimuthal angle Φ of the Fe—N_ϵ(His F8) bond.

Even though the coupling model of Friedman et al. (44) provides a reasonable and consistent description of our Raman data, it should not be overlooked that it does not describe the physical relationship between the geometric parameters of the Fe—His complex and the vibronic coupling determining the intensities of the ν_{Fe-His} sublines. This recently has been attempted in another coupling model proposed by Stavrov (61) and Bersuker and Stavrov (62). It considers that the A_{2u} orbitals of the porphyrin macrocycle and the d_{z^2}-σ_L orbitals of the Fe—N_ϵ (His F8) bond are mixed by pseudo-Jahn–Teller coupling induced by out of plane modes of A_{2u} symmetry and static distortions caused by the axial oriented proximal imidazole. In a pentacoordinated Fe-porphyrin, this interaction stabilizes the high spin configuration of iron and causes its out of plane displacement δ (63). The overlap between the above A_{2u} and A_{1g} orbitals can be shown to increase with increasing δ. Excitation into the B state changes the population of the A_{2u} orbitals, thus reducing the Fe displacement δ. As a consequence, the adiabatic potential minimum moves with respect to the ground state along the coordinate δ, giving rise to the Raman intensity of the ν_{Fe-His} mode. This model also can be used to correlate our Raman data on ν_4 and ν_{Fe-His}. Since it predicts that the frequency of the ν_{Fe-His} mode decreases with increasing δ, it relates the five sublines derived from the ν_{Fe-His} band to different Fe displacements. This also may give rise to different angles Θ (63), in accordance with Friedman's model (44). The pH-induced variations in the intensities of the sublines should be attributed to changes in the minimum position of the excited B state with respect to δ or another internal coordinate determining the normal coordinate of the ν_{Fe-His} mode (i.e., Θ and φ.)

The decrease in δ on excitation into the B state would reduce the distances N(I)—C_δ and N(III)—C_ϵ, thus giving rise to an enhancement of B_{1g}-type distortions (cf. the HLC model). In this case the minimum of the B state is shifted along a normal distortion δQ^{B1g}, and as a consequence B_{1g}-type vibronic coupling is admixed to the Raman tensor of the ν_4 mode (64). Hence, the coupling model proposed by Stavrov also predicts that an increase in $c_{es}^{B1g}(\nu_4)$ should correlate with an increase in the intensities of corresponding ν_{Fe-His} sublines in full accordance with our results.

Now we discuss some further aspects of the vibronic coupling parameters derived from the DPDs of the ν_4 mode. First, the absence of A_{2g} distortions requires some further comments. Due to the HLC model, variations in Φ should be reflected by changes of antisymmetric coupling (c_{QB}^{A2g}). Significant contributions to c_{QB}^{A2g}, however, are only provided if the azimuthal angle Φ is large (>10°) and the Fe displacement δ is small (<0.2 Å) to enable interactions between imidazole and C_α (54). Thus, the absence of A_{2g} coupling implies that these conditions are not met. This parallels findings on deoxyHb, deoxyMb (54), and deoxyHb-chironomous thummi thummi (CTT)III (65), the ν_4 mode of which shows only small contributions from A_{2g} coupling. The B_{1g} contributions to the ν_4 mode are exceptionally strong, compared with corresponding parameter values found for other heme proteins (deoxyHbA, oxyHbA, and its isolated subunits, deoxyMb). A similar finding has been made on oxyMb (54), but in this molecule B_{1g} distortions are induced by interactions between dioxygen and N(III). In the case of deoxyHb-trout IV, the large c_{es}^{B1g} suggest comparatively small values of Φ that can be expected to give rise to particular strong B_{1g} perturbations of the pyrrole nitrogens in the tilted gemometry of the Fe—His bond.

This interpretation parallels findings Friedman et al. (44) made on the ν_{Fe-His} band of a Hb from a deep sea fish, which exhibits a very low t-state affinity. They found that the corresponding ν_{Fe-His} mode exhibits an unusually strong intensity, which the authors related to a small azimuthal angles of the Fe—N_ϵ(His F8) bond. Moreover, they suspect that the distortions imposed on the heme in such a contrained geometry gives rise to the low t-state affinity. As derived from the binding isotherms of Hb-trout IV and HbA, the equilibrium constant K_T of Hb-trout IV is an order of magnitude lower than that of HbA (20, 40). The vibronic coupling parameters found for the ν_4 mode of deoxyHb-trout IV indicate that the low K_T values of Hb-trout IV also may be related to a small azimuthal angle of the Fe—N_ϵ(His F8) bond.

As shown above, allosteric coupling between Bohr groups and heme groups is much more effective in the β than in the α subunits. This parallels findings on HbA (17, 26, 29, 30, 40). In the β subunits, protonation affects the vibronic coupling parameters to a different extent. Although c_{QQ}^{A1g} significantly depends on the protonation state (i, j), c_{QB}^{A1g} and c_{BB}^{A1g} remain unaffected in the limit of accuracy. The very same finding recently has been made on deoxyHb-CTT III (66). This is contradictory to Gouterman's four-orbital model (46), which predicts

$$c_{QQ}^{A1g} = a'_{1g} - \sin(2\nu)a_{1g},$$
$$c_{QB}^{A1g} = \cos(2\nu)a_{1g},$$
$$c_{BB}^{A1g} = a'_{1g} + \sin(2\nu)a_{1g}. \qquad (11)$$

$\nu = 0.17$ is the unmixing parameter, whereas a'_{1g} and a_{1g}

describe the FC and HT coupling in the framework of the 50:50 states. Eq. 8 implies that at least variations in $c_{QQ}^{A_{1g}}$ and $c_{BB}^{A_{1g}}$ should be correlated, in contrast to our observation. Moreover, one would expect that $c_{QQ}^{A_{1g}} - c_{BB}^{A_{1g}} = (\cos 2\nu - \sin 2\nu)a_{1g}$, which is also not consistent with our data.

Two possible explanations may be given to explain this discrepancy. First, one may consider that two-electron matrix elements may contribute to $c_{QQ}^{A_{1g}}$ and $c_{BB}^{A_{1g}}$ (51). In Gouterman's two-electron picture, they would read as (51):

$$\widetilde{a_{1g}} = \langle A_{1u}E_{g\rho}|\partial^{H}/\partial Q_{1g}^{A}|A_{2u}E_{g\sigma}\rangle, \quad \rho, \sigma = x, y. \tag{12}$$

This matrix element is positive in $c_{QQ}^{A_{1g}}$ and negative in $c_{BB}^{A_{1g}}$. Therefore, if a'_{1g} and $\widetilde{a_{1g}}$ exhibit a similar dependence of the protonation state (i, j), their variations as a function of pH add up for $c_{QQ}^{A_{1g}}$ but may nearly eliminate for $c_{BB}^{A_{1g}}$. Two-electron matrix elements for vibronic coupling have been shown to exist if the electronic distributions follow the nuclei in a model for a vibrating molecule. Consideration of such "flocking basis sets" are necessary for the convergence of perturbation calculations based on the conventional Herzberg–Teller approach (66). Second, one may assume that out of plane modes of the porphyrin macrocycle are capable to vibronically couple the Q states (symmetry E_u) with the d_π states (symmetry E_g) of Fe^{2+} (π–d interaction) (67). This type of interaction would mix d_π orbitals into the Q states, thus rendering them sensitive to structural changes in the Fe—His F8 complex. At present, we believe that both π–d interactions and two-electron matrix elements contribute to vibronic coupling of the ν_4 mode. Further theoretical and experimental studies are apparently necessary to get more insight into these mechanisms.

Heme–protein coupling monitored by the DPD of the ν_{10} mode

As mentioned in the result section, the DPD of the ν_{10} mode monitors interactions that mainly result from the (asymmetric) influence of the PS on the porphyrin macrocycle. These can be modified by noncovalent interactions between the PS and the heme environment.

All RTCs can be described solely in terms of protonations of the Bohr groups in the β subunits. This suggests that the influence on the corresponding ν_{10} by proton binding to Bohr groups in the α subunits is weak. Similar findings have been obtained for oxyHbA and its isolated subunits (19, 30). The influence of heme–imidazole coupling on the ν_{10} mode is expected to be weak for reasons given in Results. As a consequence, there is no strict correlation between the $c_{es}^{\Gamma}(\nu_{10})$ and the intensities of the ν_{Fe-His} sublines. Moreover, in contrast to what has been obtained for ν_4, no unique correlation between the $c_{es}^{\Gamma}(\nu_{10})$ exists. The parameter $c_{QB}^{B_{1g}}$, which depends on A_{1g} distortions, and parameter $c_{QB}^{A_{1g}}$ (reflecting B_{1g} distortions) exhibit $c_{es}^{\Gamma}(1.1) \gg c_{es}^{\Gamma}(1.0) + c_{es}^{\Gamma}(0.1) > c_{es}^{\Gamma}(0.0)$, whereas the remaining parameters (i.e., $c_{QQ}^{A_{1g}}$ and $c_{BB}^{A_{1g}}$) correlate with the c_{es}^{Γ} of the ν_4 mode.

The PS may influence the porphyrin macrocycle directly or in an indirect way. The direct coupling includes electron withdrawing from the A_{1u} orbitals of C_β atoms by the carbon hydrogen chains of the PS (68). The different PS can be expected to differ in terms of their electron withdrawing capacity, thus giving rise to asymmetric distortions of the pyrroles. As shown by Schweitzer-Stenner et al. (30), one expects B_{2g} and A_{2g} distortions if identical PS cause the same distortions. Our data clearly show, however, that A_{1g} coupling is admixed to the Raman tensor of the ν_{10} mode that results from B_{1g} distortions. Thus, some of the identical PS interact differently with the C_β. Ideal candidates for this are the two vinyls attached to the pyrroles II and III (V(II) and V(III)) for the following reasons. First, there is some electronic mixing between the exited states Π^* states of the vinyls and the porphyrins (69). Second, it is known that V(II) and V(III) have different orientations with respect to heme in deoxy- and oxyHbA (3, 70, 71), which can be expected to cause different distortions of the corresponding C_β. Third, V(III) exhibits a van der Waals bond to Val FG4 β that is located close to the amino acids that may be involved in the β subunit Bohr effect, namely Ser F9 β and Glu FG1 β (72), which are H-bonded to the carboxyl group and the imidazole of the COOH-terminal His HC3 β. Furthermore, it is known that Val FG5 β is H-bonded to the penultimate Tyr HC2 β (12, 14, 70), which is most probably also the case in Hb-trout IV. This H-bond serves as a direct linkage between the COOH-terminal His HC3 β and the flexible FG-helix and is of utmost importance for the R-state Bohr effect in oxyHbA (19). One may therefore expect that the protonation of Bohr groups in the β subunit rearranges the structure close to His F8 and Val FG5, thus giving rise to changes in the orientation of the proximal imidazole and V(III). The latter is then reflected by the RTCs of the ν_{10} mode.

An indirect influence of the PS on the structure of the macrocycle may be caused by noncovalent PS–PS interactions that have been shown to cause strong nonplanar distortions of metalloporphyrins in solution (73, 74), thus lowering their symmetry from D_{4h} to D_{2d} or S_4 (52). Since the PS are not equivalent, these distortions would be asymmetric and the symmetry of the macrocycle would be lowered further to C_2 or C_s. The nonplanarity depends on the length of the PS and on their orientation with respect to each other. Changes of the latter may therefore cause changes in nonplanarity and thus variations of the DPD of the ν_{10} mode. Support for this model comes from the dispersion experiments on the isolated subunits of oxyHbA (30), which showed that asymmetric perturbations affect the ν_{10} mode in β^{SH}-oxyHb rather than in α^{SH}-oxyHbA. Crystallographic data on the intact oxyHbA had previously revealed that the macrocycle in

the α subunits is planar, whereas it exhibits significant tilting of its pyrroles in the β subunit (70).

SUMMARY

Raman dispersion experiments on deoxyHb-trout IV have shown that proton binding to Bohr groups causes considerable asymmetric distortions of the heme groups. This process of heme–protein coupling is much more pronounced in the β than in the α subunits. It involves heme–protein interactions between the proximal His F8 and the pyrrole nitrogens and noncovalent binding between the FG helix in the β subunit and the PS of the prosthetic heme group. It could be shown further that the pH dependence of the vibronic-coupling parameters of the ν_4 mode correlate nicely with the pH-dependent variations in the intensities of the sublines into which the ν_{Fe-His} band profile was recently decomposed (41). This finding can be explained by two different coupling models designed to explain the resonance enhancement of the ν_{Fe-His} mode in the B-band region.

R. Schweitzer-Stenner thanks Dr. Solomon Stavrov for helpful discussions on vibronic coupling processes in Fe-porphyrins.

We gratefully acknowledge the support by a grant from the Deutsche Forschungsgemeinschaft.

Received for publication and in final form 6 August 1992.

REFERENCES

1. Szabo, A., and M. Karplus. 1975. Analysis of cooperativity in hemoglobin. Valency hybrids, oxidation and methemoglobin replacement reactions. *Biochemistry.* 14:931–1940.
2. Herzfeld, J., and E. Stanley. 1974. A general approach to cooperativity and its application to oxygen equilibrium of hemoglobin and its effectors. *J. Mol. Biol.* 82:231–265.
3. Gellin, B., and M. Karplus. 1977. Mechanism of tertiary structural change in hemoglobin. *Proc. Natl. Acad. Sci. USA.* 74:801–805.
4. Baldwin, J. L., and C. Chotia. 1979. Haemoglobin, the structural changes related to ligand binding and its allostreric mechanism. *J. Mol. Biol.* 129:175–200.
5. Johnson, M. L., and G. K. Ackers. 1982. Thermodynamic analysis of human hemoglobins in terms of the Perutz mechanism: extensions of the Szabo-Karplus model to include subunit assembly. *Biochemistry.* 21:201–211.
6. Friedman, J. M. 1985. Structure, dynamics and reactivity in hemoglobin. *Science (Wash. DC).* 228:1274–1280.
7. Ackers, G. K., and F. R. Smith. 1986. Resolving pathways of functional coupling within protein assemblies by site specific structural perturbation. *Biophys. J.* 49:155–165.
8. Murray, L. P., J. Hofrichter, E. R. Henry, and W. A. Eaton. Time resolved optical spectroscopy and structural dynamics following photodissociation of carbonmonoxy hemoglobin. *Biophys. Chem.* 29:63–76.
9. Rousseau, D. L., and J. M. Friedman. 1988. Transient and cryogenic studies of photodissociated hemoglobin and myoglobin. *In* Biological Application of Raman Spectroscopy. T. G. Spiro, editor. John Wiley & Sons Inc., New York/Chichester. 133–216.
10. Lee, A. W., M. Karplus, C. Poyart, and E. Bursaux. 1988. Analysis of Proton Release in Oxygen Binding by Hemoglobin: Implication for the Cooperative Mechanism. *Biochemistry.* 27:1285–1301.
11. Eaton, W. A., E. R. Henry, and J. Hofrichter. 1991. Application of linear free energy relations to protein conformational changes: the quaternary structural change of hemoglobin. *Proc. Natl. Acad. Sci. USA.* 88:4472–4475.
12. Perutz, M. F. 1989. Mechanism of cooperativity and allosteric regulation in proteins. *Q. Rev. Biophys.* 22:139–236.
13. Zhang, M., F. A. Ferrone, and A. J. Martino. 1990. Allosteric kinetics and equilibria differ for carbon monoxide and oxygen binding to hemoglobin. *Biophys. J.* 58:333–340.
14. Perutz, M. F. 1970. The Bohr effect and combination with organic phosphates. *Nature (Lond.).* 228:734–739.
15. Kilmartin, J. V., J. H. Fogg, and M. F. Perutz. 1980. Role of C-terminal histidine in the alkaline Bohr effect of human hemoglobin. *Biochemistry.* 19:3189–3193.
16. Wyman, J., J. Gill, H. T. Gaud, A. Colosimo, B. Giardina, H. A. Kuiper, and M. Brunori. 1978. Thermodynamics of ligand binding and allosteric transitions in hemoglobins. Reaction of Hb trout IV with CO. *J. Mol. Biol.* 124:161–175.
17. Scott, T. W., J. M. Friedman, M. Ikeda-Saito, and T. Yonetari. 1983. Subunit heterogeneity in the structure and dynamics of hemoglobin. A transient Raman study. *FEBS (Fed. Eur. Biochem. Soc.) Letts.* 158:68–71.
18. Kwiatkowski, L., and R. W. Noble. 1982. The contribution of histidine (HC3) (146 β) to the R-state Bohr effect of human hemoglobin. *J. Biol. Chem.* 257:8891–8895.
19. Schweitzer-Stenner, R., D. Wedekind, and W. Dreybrodt. 1986. Correspondence of the pK-values of oxyHb-titration states detected by resonance Raman scattering to kinetic data of ligand dissociation and association. *Biophys. J.* 49:1077–1088.
20. Schweitzer-Stenner, R. 1989. Allosteric linkage-induced distortions of the prosthetic group in haem proteins as derived by the theoretical interpretation of the depolarization ratio in resonance Raman scattering. *Q. Rev. Biophys.* 22:381–479.
21. Warshel, A. 1977. Energy-structure correlations in metalloporphyrins and the control of oxygen binding by hemoglobin. *Proc. Natl. Acad. Sci. USA.* 74:1789–1793.
22. Ten Eyck, L. F. 1979. Hemoglobin and myoglobin. *In* The Porphyrins. Vol. III. D. Dolphin, editor. Academic Press, New York. 445–472
23. Collins, D. W., P. Champion, and D. B. Fitchen. 1976. Resonant Raman scattering from heme proteins. Polarization dispersion and α-band splitting. *Chem. Phys. Letts.* 40:416–420.
24. Schweitzer-Stenner, R., W. Dreybrodt, and S. el Naggar. 1984. Investigation of pH-induced symmetry distortions of the prosthetic group in deoxyhemoglobin by resonance Raman scattering. *Biophys. Struct. Mech.* 10:241–256.
25. Shih, T. B., R. T. Jones, J. Bonaventura, and C. Bonaventura. 1984. Involvement of His HC3(146)β in the Bohr effect of human hemoglobin. Studies of native and N-ethyl-maleimido-treated hemoglobin A and hemoglobin cowtown (β146His → Leu). *J. Biol. Chem.* 259:967–974.
26. Wedekind, D., R. Schweitzer-Stenner, and W. Dreybrodt. 1985. Heme-apoprotein interaction in the modified oxyhemoglobin-bis(N-maleimidomethyl)ether and in oxyhemoglobin at high Ci-concentration detected by resonance Raman scattering. *Biochim. Biophys. Acta.* 830:224–232.
27. Wedekind, D., U. Brunzel, R. Schweitzer-Stenner, and W. Dreybrodt. 1986. Correlation of pH-dependent resonance Raman and optical absorption data reflecting haem-aproprotein interaction in oxyhemoglobin. *J. Mol. Struct.* 143:457–460.
28. Schweitzer-Stenner, R., D. Wedekind, and W. Dreybrodt. 1989. The influence of structural variations in the F- and FG-helix of the β-subunit modified oxyHb-NES on the heme structure de-

tected by resonance Raman spectroscopy. *Eur. Biophys. J.* 17:87–100.

29. Chavez, M. D., S. H. Courtney, M. R. Chance, D. Kiula, J. Nocek, B. M. Hofman, and J. M. Friedman. 1990. Structural and functional significance of inhomogenous line broadening of band III in hemoglobin and Fe — Mn hybrid hemoglobin. *Biochemistry.* 29:4844–4852.
30. Schweitzer-Stenner, R., U. Dannemann, and W. Dreybrodt. 1992. Investigation of Heme Distortions and Heme-Protein Coupling in the Isolated Subunits of Oxygenated Human Hemoglobin by Resonance Raman Dispersion Spectroscopy. *Biochemistry.* 31:694–702.
31. Wyman, J. 1966. Allosteric linkage. *J. Am. Chem. Soc.* 89:2202–2218.
32. Ascoli, T. G., B. Falcioni, B. Giardina, and M. Brunori. 1986. Thermodynamic characterization of the allosteric transition in trout hemoglobin. *E. Biophys. J.* 13:245–249.
33. Antonini, E., and M. Brunori. 1970. Hemoglobin and Myoglobin in their Reaction with Ligands. Elsevier, Amsterdam. 175–183.
34. Moffat, J. K. 1971. Structural and functional properties of chemically modified horse hemoglobin. *J. Mol. Biol.* 58:79–88.
35. El Naggar, S., W. Dreybrodt, and R. Schweitzer-Stenner. 1985. Haem-protein interactions detected by resonance Raman scattering in Mb- and Hb-derivates lacking the saltbridge His 146b-Asp94b. *Eur. Biophys. J.* 12:43–49.
36. El Naggar, S., R. Schweitzer-Stenner, W. Dreybrodt, and A. Mayer. 1984. Determination of the Raman Tensor of the Haem Group in Myoglobin by Resonance Raman Scattering in Solution and Single Crystals. *Biophys. Struct. Mech.* 10:257–273.
37. Brunori, M. 1975. Molecular adaption to biophysical requirements. *Curr. Top. Cell. Regul.* 9:1–39.
38. Brunori, M., M. Coletta, B. Giardina, and J. Wyman. 1978. A macromolecular transducer as illustrated by trout hemoglobin IV. *Proc. Natl. Acad. Sci. USA.* 75:4310–4312.
39. Schweitzer-Stenner, R., and W. Dreybrodt. 1989. An extended Monod–Wyman–Changeaux model expressed in terms of the Herzfeld–Stanley formalism applied to oxygen and carbon monoxide binding curves of hemoglobin trout IV. *Biophys. J.* 55:691–701.
40. Schweitzer-Stenner, R., D. Wedekind, and W. Dreybrodt. 1989. Detection of heme perturbations caused by the quaternary R → T transition in oxyhemoglobin trout IV by resonance Raman scattering. *Biophys. J.* 55:703–712.
41. Bosenbeck, M., R. Schweitzer-Stenner, and W. Dreybrodt. 1992. pH-induced conformational changes of the Fe^{2+} — N_ϵ(His F8) linkage in deoxyhemoglobin trout IV detected by the Raman active Fe^{2+} — N_ϵ(His F8) stretching mode. *Biophys. J.* 61:31–41.
42. Kitagawa, T. 1988. Heme protein structure and the iron histidine stretching mode. *In* Biological Application of Raman Spectroscopy. T. G. Spiro, editor. John Wiley & Sons Inc. New York/Chichester. 97–132.
43. Bangcharoenpaurpong, O., K. T. Schomaker, and P. Champion. 1984. A resonance Raman investigation of myoglobin. *J. Am. Chem. Soc.* 106:5688–5698.
44. Friedman, J. M., B. F. Campbell, and R. W. Noble. 1990. A possible new control mechanism suggests by resonance Raman spectra from a deep ocean fish hemoglobin. *Biophys. Chem.* 37:43–59.
45. Loudon, R. 1979. Quantum Theory of Light. Clarendon Press, New York.
46. Gouterman, M. 1959. Study of the effects of substitution on the absorption spectra of porphyrin. *J. Chem. Phys.* 30:1139–1161.
47. Shelnutt, J. A. 1981. The Raman excitation spectra and absorption spectrum of a metalloporphyrin in an environment of low symmetry. *J. Chem. Phys.* 72:3948–3958.
48. Placzek, G. 1934. Rayleighstreuung und Ramaneffekt. *In* Handbuch der Radiologie, Bd. 6. E. Marx, editor. Akademische Verlagsanstalten, Leipzig.
49. Spiro, T. G., and T. C. Strekas. 1974. Resonance Raman spectra of heme proteins: effects of oxidation and spin state. *J. Am. Chem. Soc.* 96:338–345.
50. Bobinger, U., R. Schweitzer-Stenner, and W. Dreybrodt. 1989. Highly resolved depolarization ratio dispersion and excitation profiles of Raman fundamentals of protoporphyrin IX in a heme protein matrix. *J. Raman Spectrosc.* 20:191–201.
51. Schweitzer-Stenner, R., U. Bobinger, and W. Dreybrodt. 1991. Multimide Analysis of Depolarization Ratio Dispersion and Excitation Profiles of Seven Raman Fundamentals from the Haem Group in Ferrocytochrome c. *J. Raman Spectrosc.* 22:65–78.
52. Bobinger, U., R. Schweitzer-Stenner, and W. Dreybrodt. 1991. Investigation of asymmetric perturbations of Ni(II)-octaethylporphyrin in CH_2Cl_2 by Raman dispersion spectroscopy. *J. Phys. Chem.* 95:7625–7634.
53. Li, X.-Y., R. S. Czersnuszewicz, J. R. Kincaid, P. Stein, and T. G. Spiro. 1990. Consistent Porphyrin Force Field. 2. Nickel Octaethylporphyrin Skeletal and Substituent Mode Assignments from ^{15}N, Meso-d_4, and Methylene-d_{16} Raman and Infrared Isotope Shifts. *J. Phys. Chem.* 94:47–61.
54. Schweitzer-Stenner, R., and W. Dreybrodt. 1992. Investigation of Haem Protein Coupling and Structural Heterogenity in Myoglobin and Haemoglobin by Resonance Raman Spectroscopy. *J. Raman Spectrosc.* 23:539–550.
55. Bosenbeck, M. 1990. Resonanz-Raman-Streuung an Hämoglobin der Forelle *salmo irideus.* Dr. rer. nat. Dissertation. University of Bremen, Germany. 33–37.
56. Srajer, V., K. T. Schomaker, and P. M. Champion. 1986. Spectral broadening in biomolecules. *Phys. Rev. Lett.* 57:1267–1270.
57. Cordone, L., A. Cupane, M. Leone, and E. Vitrano. 1986. Optical absorption spectra of deoxy- and oxyhemoglobin in the temperature range 300–20 K. Relation with protein dynamics. *Biophys. Chem.* 24:259–275.
58. Srajer, V., L. Reinish, and P. M. Champion. 1988. Protein fluctuations, distributed coupling, and the binding of ligands to heme proteins. *J. Am. Chem. Soc.* 110:6656–6666.
59. Ondrias, M. R., D. L. Rousseau, J. A. Shelnutt, and S. R. Simon. 1982. Quaternary transformation induced changes at the heme in deoxyhemoglobins. *Biochemistry.* 21:3420–3437.
60. Ahmed, A. M., B. F. Campbell, D. Caruso, M. R. Chance, M. D. Chavez, S. H. Courtney, J. M. Friedman, I. E. T. Iben, M. R. Ondrias, and M. Yang. 1991. Evidence for proximal control of ligand specificity in hemeproteins: absorption and Raman studies of cyrogenically trapped photoproducts of ligand bound myoglobin. *Chem. Phys.* 158:329–351.
61. Stavrov, S. A. 1992. The contribution of the out-of-plane iron displacement to the strong coupling of the Fe — His(F8)-mode in the resonance region of the Soret band. *Proc. Symp. Raman Spectrosc. Biol. Syst. Bremen.* 19.
62. Bersuker, I. B., and S. S. Stavrov. 1988. Structure and Properties of Metalloporphyrins and Hemproteins: The Vibronic Approach. *Coord. Chem. Rev.* 88:1–68.
63. Powers, L., B. Chance, M. Chance, B. Campbell, J. M. Friedman, S. Khalid, C. Kumar, A. Naqui, K. S. Reddy, and Y. Zhou. 1987. Kinetic, Structural and Spectroscopic Identification of Geminate States of Myoglobin: A Ligand Site on the Reaction Path. *Biochemistry.* 26:4785–4796.
64. Tsuboi, M., and A. Hirakawa. 1976. Adiabatic potential and Raman scattering: a theoretical background for a proposed rule. *J. Raman Spectrosc.* 5:76–86.

65. Jentzen, W., W. Dreybrodt, R. Schweitzer-Stenner, and K. Gersonde. 1990. Heme distortions in monomeric insect Hb-CTT III: resonance Raman scattering and its relation to biological function. *Proc. XII Int. Conf. Raman Spectrosc.* Columbia University Press, New York. 680–681.

66. Curtis, W. C., and O. E. Weigang. 1975. Theory of vibronic interactions. The importance of floating basis sets. *J. Chem. Phys.* 63:2135–2143.

67. Mineyev, A. P., Y. A. Sharanov, N. A. Sharanova, and Y. P. Lysov. 1983. p-d-Interaction and the Temperature Dependent Magnetic Circular Dichroism Spectra of Low Spin Fe(III)—Heme Compounds. *Theor. Chim. Acta.* 65:421–438.

68. Shelnutt, J. A., and V. Ortiz. 1985. Substituent Effects on the Electronic Structure of Metalloporphyrins: A Quantitative Analysis in Terms of Four Orbital Model Parameters. *J. Phys. Chem.* 89:4733–4739.

69. DeVito, V. L., and S. A. Asher. 1989. UV-resonance enhancement of vinyl stretch in ferric protoporphyrin IX: conjugation or preservation of the vinyl $\pi \rightarrow \pi^*$ transitions. *J. Am. Chem. Soc.* 26:9143–9156.

70. Shaanan, B. 1983. Structure of human oxyhemoglobin at 2.1 Å resolution. *J. Mol. Biol.* 171:31–59.

71. Fermi, G., M. F. Perutz, B. Shaanan, and R. Fourme. 1984. Human deoxyhaemoglobin at 1.74 Å resolution. *J. Mol. Biol.* 175:159–174.

72. Perutz, M. F., and M. Brunori. 1982. Sterochemistry of cooperative effects in fish and amphibian hemoglobin. *Nature (Lond.).* 299:241–426.

73. Shelnutt, J. A., C. J. Medforth, M. D. Barber, K. M. Barkigia, and K. M. Smith. 1991. Relationship between structural parameters and Raman frequencies for some planar and nonplanar Nickel (II) Porphyrins. *J. Am. Chem. Soc.* 113:4077–4087.

74. Shelnutt, J. A., J. D. Hobbs, S. A. Majumder, L. D. Sparks, C. J. Medforth, M. O. Senge, K. M. Smith, M. Miura, and H. M. E. Quirke. 1992. Resonance Raman Spectroscopy of Non-Planar Nickel Porphyrins. *J. Raman Spectrosc.* 23:523–529.